

Article

Electrochemical Deposition and Properties of Ni Coatings with Nitrogen-Modified Graphene Oxide

Vitaly Tseluikin ^{*}, Asel Dzhumieva , Alena Tribis, Sergey Brudnik , Denis Tikhonov, Andrey Yakovlev , Anton Mostovoy  and Marina Lopukhova

Engels Technological Institute, Yuri Gagarin State Technical University of Saratov, Polytechnicheskaya St., 77, 410054 Saratov, Russia; aselka2796@gmail.com (A.D.); tribis2004@mail.ru (A.T.); sbrud@mail.ru (S.B.); tikhonov-denis@mail.ru (D.T.); aw_71@mail.ru (A.Y.); mostovoy19@rambler.ru (A.M.); mlopuhova@yandex.ru (M.L.)

* Correspondence: tseluikin@mail.ru

Abstract: In this study, a method for producing nitrogen-modified graphene oxide (NMGO) using hydrothermal synthesis in the presence of triethanolamine is presented. The composition and structure of NMGO are characterized using X-ray phase analysis (XPA), scanning electron microscopy (SEM), Fourier transform infrared spectroscopy, and Raman spectroscopy. Ni-based metal matrix coatings (MMCs) modified with NMGO were obtained from a sulfate-chloride electrolyte in the galvanostatic mode. The process of electrochemical deposition of these coatings was studied using chronovoltammetry. The microstructure of Ni–NMGO MMCs was studied using the XPA and SEM methods. It has been established that the addition of NMGO particles into the Ni matrix results in an increase in the microhardness of the resulting coatings by an average of 1.30 times. This effect is a consequence of the refinement of crystallites and high mechanical properties of NMGO phase. The corrosion-electrochemical behavior of studied electrochemical deposits in 0.5 M sulfuric acid was analyzed. It has been shown that the corrosion rate of Ni–NMGO MMCs in a 3.5% sodium chloride environment decreases by approximately 1.50–1.70 times as compared to unmodified Ni coatings. This is due to NMGO particles that act as a barrier preventing the propagation of the corrosion and form corrosive galvanic microelements with Ni, promoting anodic polarization.

Keywords: metal matrix coatings; nitrogen-modified graphene oxide; electrodeposition; structure; microhardness; corrosion



Citation: Tseluikin, V.; Dzhumieva, A.; Tribis, A.; Brudnik, S.; Tikhonov, D.; Yakovlev, A.; Mostovoy, A.; Lopukhova, M. Electrochemical Deposition and Properties of Ni Coatings with Nitrogen-Modified Graphene Oxide. *J. Compos. Sci.* **2024**, *8*, 147. <https://doi.org/10.3390/jcs8040147>

Academic Editor: Andrey Chumaevskii

Received: 7 February 2024

Revised: 21 March 2024

Accepted: 11 April 2024

Published: 13 April 2024



Copyright: © 2024 by the authors. Licensee MDPI, Basel, Switzerland. This article is an open access article distributed under the terms and conditions of the Creative Commons Attribution (CC BY) license (<https://creativecommons.org/licenses/by/4.0/>).

1. Introduction

Electrochemical deposition of coatings based on Ni and its alloys is one of the common methods for modifying the surface of steel products to protect them from wear and corrosion [1]. A significant improvement in the characteristics of electrolytic nickel can be achieved by its co-deposition with various dispersed particles. Electrochemical deposits modified with the dispersed phase are called composite or metal matrix coatings (MMCs). Ni-based MMCs have an excellent adhesive properties, high hardness, abrasive resistance, and can be used in mechanical engineering, chemical and oil and gas industries, medical equipment, etc. [2–4].

Properties of metal matrix coatings are largely determined by the dispersed phase. Among the variety of dispersed materials, carbon derivatives attract the considerable attention of researchers. In particular, nickel MMCs modified with carbon nanotubes [5–7], fullerenes [8,9], nanodiamonds [10,11], and graphene and its oxide [12–17] have been obtained. The latter occupy a special place among carbon compounds. Graphene is a two-dimensional material with a high specific surface area. When it reacts with strong mineral acids, graphene oxide (GO) is formed. The synthesis of new graphene and graphene oxide derivatives, as well as their study, remain urgent tasks, and represent undoubted scientific novelty and significance in connection with the prospects for their practical use. For

example, as supercapacitors [18,19], for batteries and fuel cells [20,21], and hypersensitive sensors [22]. GO and its modified analogues are used as reinforcing additives in polymer materials and cements [23,24], in biological and biomedical applications [25], etc.

In the GO structure, carbon atoms are bonded to oxide functional groups (carbonyl, carboxyl, epoxy, etc.), due to which it is hydrophilic and forms stable aqueous dispersions. These compounds are inert in many aggressive environments, which makes them suitable for corrosion protection [26–28]. Therefore, modifying graphene oxide with various agents, particularly nitrogen, to enhance its anticorrosion ability is of great interest.

For this purpose, various nitrogen-containing organic compounds can be used, among which triethanolamine (TEA) is the most notable. This compound is one of the class of amino alcohols; it is a low-toxic and relatively cheap chemical reagent that can be used as a corrosion inhibitor in various corrosive environments [29–31]. TEA is highly reactive due to the presence of polar tertiary amine functional groups and alcohol hydroxyl groups in the molecule. Inhibition of the TEA corrosion process occurs due to the chemical interaction of TEA functional groups on the metal surface or through electrostatic interactions [32]. In this regard, TEA can act as a modifying agent for nitrogen functionalization of the GO surface. Therefore, one should expect that nitrogen-modified graphene oxide (NMGO), when included in the matrix of electrochemical deposits, will help improve their performance characteristics.

The purpose of this work is to deposit metal-matrix coatings based on nickel with the dispersed NMGO phase under stationary electrolysis conditions (galvanostatic mode), and to study the microstructure, physical-mechanical, and corrosion properties of these MMCs.

2. Materials and Methods

(a) Modification of GO

GO was synthesized electrochemically according to the procedure described in [33]. Electrochemical oxidation of graphite was carried out in galvanostatic mode with a current of 0.4 A, in 83% sulfuric acid with subsequent hydrolysis of oxidized graphite to pH 6 for 1 h and dried at a temperature of 90 °C. The resulting GO (0.1 g) was dispersed in 100 mL of distilled water under ultrasonication for 2 h. After this, the dispersed GO and 10 mL of triethanolamine were carried into a fluoroplastic liner which was placed into a steel autoclave. Hydrothermal synthesis proceeded for 20 h at 180 °C. The resulting nitrogen-modified graphene oxide (NMGO) was washed with 250 mL of distilled water and dried at 80 °C for 10 h (Figure 1). The hydrothermal method of graphene oxide modification with triethanolamine has also been used in [32].

(b) Electrodeposition of Ni coatings

Ni–NMGO metal matrix coatings were deposited onto a steel substrate (45 steel) from a Watts-type sulfate-chloride electrolyte (Table 1). The substrate (cathode) was positioned vertically.

Table 1. Electrolyte bath composition and electrolysis parameters.

Electrolyte Bath	Concentration, g/L	Deposition Parameters
NiSO ₄ ·7H ₂ O	220	Temperature $t = 45$ °C, pH ≈ 4.5 Constant stirring Cathode current densities $i_c = 7, 8, 9, 10$ A/dm ²
NiCl ₂ ·6H ₂ O	40	
CH ₃ COONa	30	
NMGO	1	

The NMGO powder was dispersed in the electrochemical cell before starting the deposition process. Electrochemical coatings with pure nickel were prepared from the above-mentioned solution without the dispersed NMGO phase. The thickness of coatings was 20 μ m. Preliminary preparation of the specimen surface included mechanical cleaning with sandpaper, anodic etching in 48% phosphoric acid with a lead counter electrode, and washing in bi-distilled water.

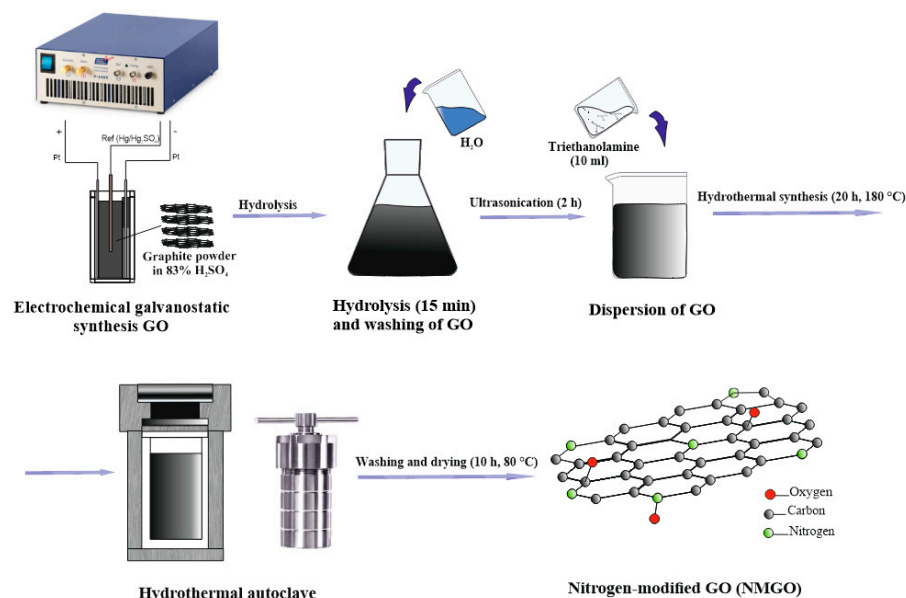


Figure 1. Scheme of nitrogen-modified graphene oxide synthesis.

(c) Study of structure and properties

To record diffraction patterns, the ARL X'TRA device (Thermo Scientific, Ecublens, Switzerland) was used by applying $\text{CuK}\alpha$ radiation ($\lambda = 0.15412 \text{ nm}$). Diffraction patterns were recorded in the 2θ range from 5° to 50° at a scanning speed of $2^\circ/\text{min}$. Operating mode of the X-ray tube: voltage $U = 40 \text{ kV}$, electric current $I = 40 \text{ mA}$. The phase analysis of the samples was performed in the PDMS software package using the international database of diffraction standards ICDD PDF-2 Release 2014.

The surface and microstructure of particles of nitrogen-modified graphene oxide, as well as nickel coatings, were studied using a scanning electron microscope (SEM) with a built-in energy-dispersive analyzer Explorer (ASPEX, Framingham, MA, USA).

Fourier transform infrared spectroscopy (FTIR) was performed using FT-801 FTIR spectrometer (Simex, Novosibirsk, Russia) in the range of $4000\text{--}500 \text{ cm}^{-1}$ at a temperature of 20°C .

Raman spectra were recorded using a spectrometer with a DXR Raman Microscope confocal microscope (Thermo Fisher Scientific, Waltham, MA, USA). A laser line with a wavelength of 532 nm was used as an excitation source. To record the spectra the exposure time of 60 s was used at power of 1% .

Electrochemical measurements were performed using a P-30J potentiostat (Elins, Moscow, Russia) with a three-electrode cell. The potentials were set relative to a saturated silver chloride reference electrode and then recalculated using a standard hydrogen electrode.

Vickers microhardness (HV) was measured using the PMT-3 device (JSC LOMO, Saint-Petersbourg, Russia), by static pressing a tetrahedral diamond pyramid with an angle of 136° into electrolytic nickel coatings under a load of 100 g .

The corrosion-electrochemical behavior of nickel coatings was assessed by the nature of the anodic potentiodynamic curves in 0.5 M sulfuric acid (potential sweep rate $V_p = 8 \text{ mV/s}$). Studies of the corrosion rate were carried out in a 3.5% sodium chloride solution.

3. Results and Discussion

3.1. Structural Studies of NMGO

The dispersed phase of various natures can electrochemically co-precipitate with nickel. The properties of the resulting metal-matrix coatings are largely determined by the structure of the particles embedded in nickel. Figure 2 shows the X-ray diffraction

(XRD) pattern of NMGO. A signal is recorded on the X-ray image with a maximum peak at $2\theta = 26.41^\circ$. However, the basal GO peak at 11.86° is absent on the XRD of NMGO.

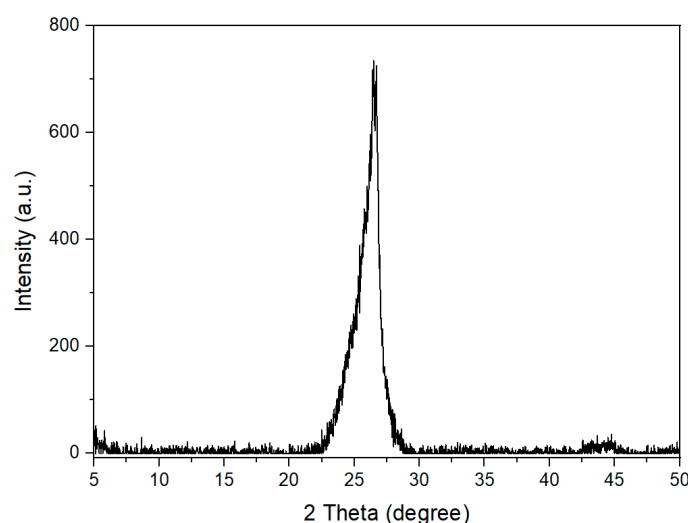


Figure 2. XRD patterns of GO modified with triethanolamine.

The IR spectrum of NMGO (Figure 3a) shows peaks of stretching vibrations of $-\text{CH}_2-$ at 2900 and 2880 cm^{-1} , and stretching vibrations of the N-H fragment at 1572 cm^{-1} . The vibration intensity of the C=C fragment at 1602 cm^{-1} decreases. The low-intensity peak of the epoxy functional group shifts to 986 cm^{-1} , which indicates partial interaction of TEA with the epoxy group.

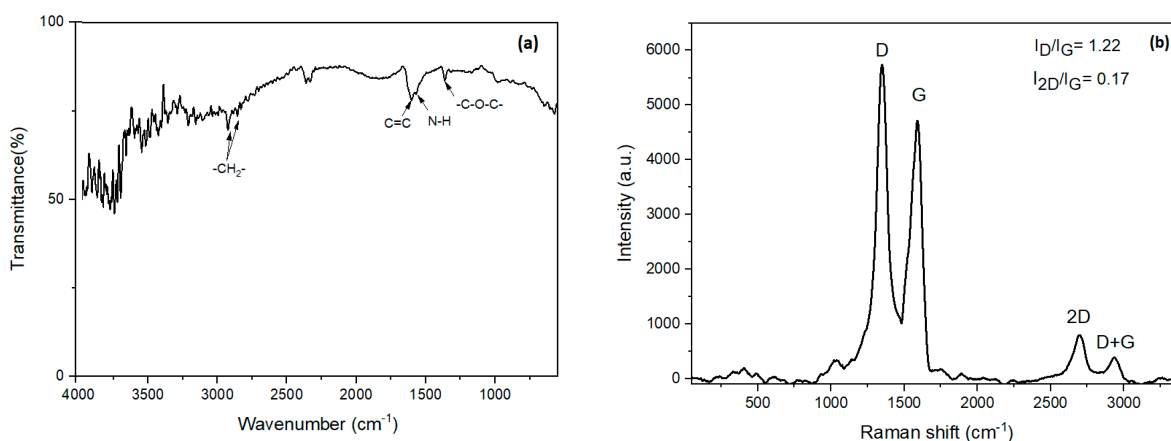


Figure 3. FT-IR (a) and RAMAN (b) spectrum of GO modified with triethanolamine.

In the Raman spectrum of NMGO (Figure 3b), a shift of the peaks is observed; there is a D band with a peak maximum of 1350 cm^{-1} and a G band with a maximum of 1584 cm^{-1} . The G band of NMGO is shifted towards lower wave numbers, which confirms the presence of defects in the graphene layers as a result of the removal of oxygen and restoration of the graphene plane [34]. The band intensity ratio is $I_D/I_G = 1.22$. The presence of a shoulder peak to the right of the G-band 2D peak in NMGO is due to the presence of defective graphite structures formed during hydrothermal modification processes. The shape of the spectrum and the observation of 2D and D+G peaks show that the particles are composed of more than two layers of NMGO.

It can be assumed that during hydrothermal modification of GO with triethanolamine, partial reduction of multilayer graphene oxide occurs, since the presence of surface oxygen groups contributes to the particle agglomeration. Studies using the SEM method

(Figure 4a,b) allow us to establish that micrographs of NMGO exhibit deformed planes of carbon particles (such effects are shown by red arrows). This leads to an increase in the concentration of surface defects on which water is likely to be adsorbed.

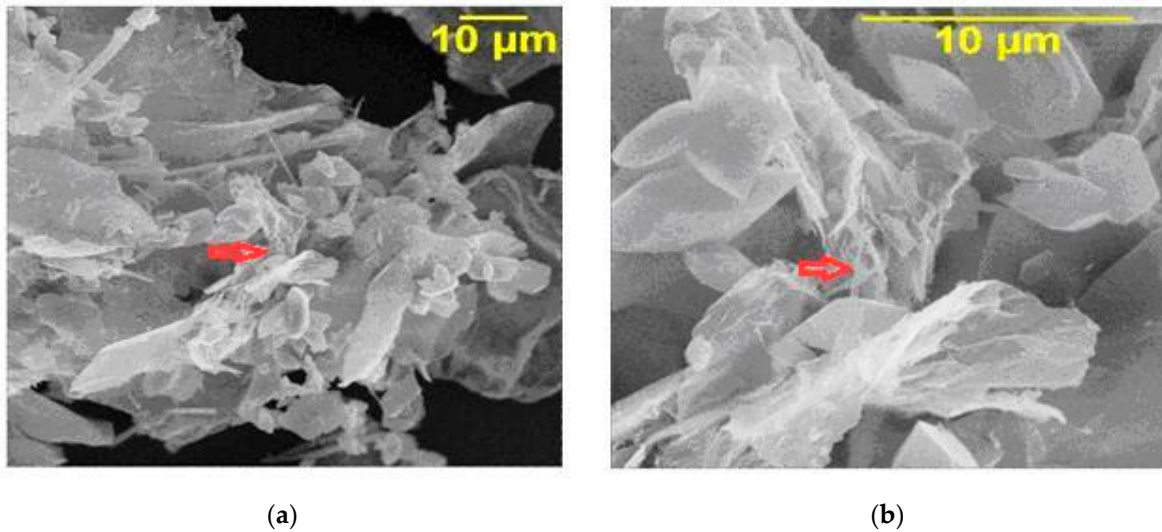


Figure 4. SEM images of GO modified with triethanolamine (magnification $\times 2500$ (a), $\times 10,000$ (b)).

3.2. Electrodeposition of Ni Coatings

The addition of powder of the NMGO dispersed phase into a Watts-type sulfate-chloride nickel plating electrolyte (Table 1) significantly affects the rate of cathode reactions. In the presence of nitrogen-modified graphene oxide, the chronovoltammogram shifts toward less-negative potentials (Figure 5). Accordingly, the deposition currents of Ni–NMGO MMCs increase compared to pure nickel, which indicates an increase in the speed of the electrode process.

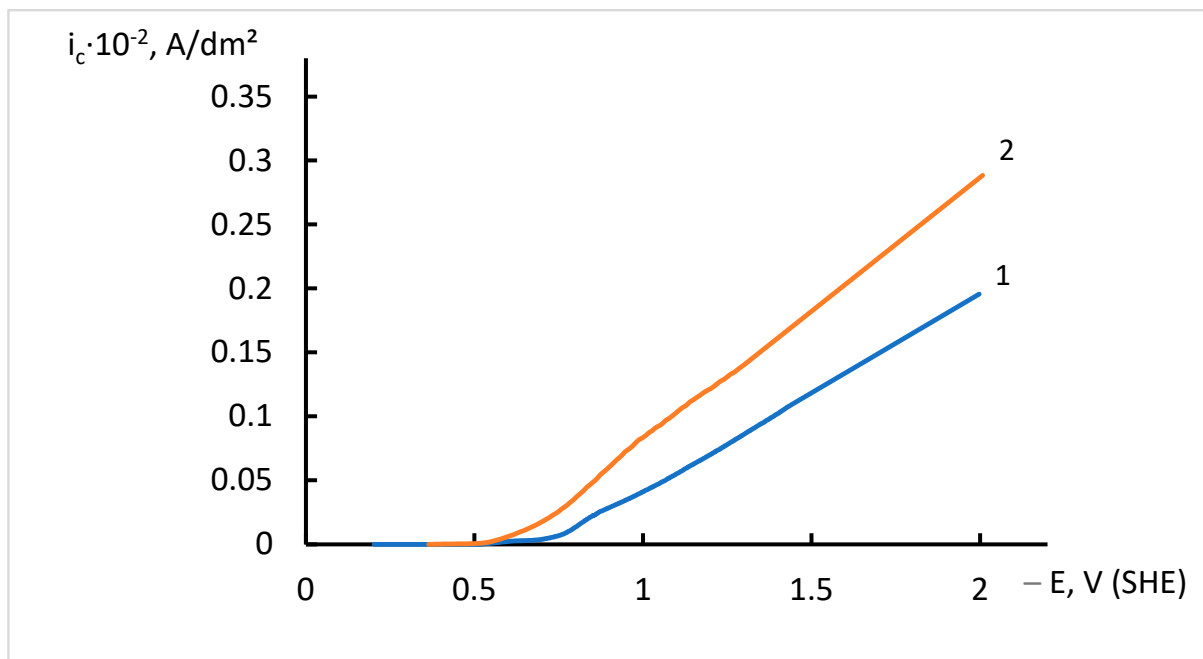


Figure 5. Chronovoltammograms of Ni (1), and Ni–NMGO MMC (2) electrochemical deposition (potential sweep rate $V_p = 8$ mV/s).

It is likely that the addition of NMGO particles into the coating occurs through two mechanisms. Firstly, due to the convection mixing of the electrolyte, the dispersed phase is brought to the cathode, captured by the growing coating, and penetrates into the intercrystalline space of the Ni matrix. Secondly, electrolyte cations can be adsorbed on the surface of NMGO, which contributes to the electrophoretic transfer of particles because of the potential gradient and their subsequent embedding into the Ni deposit.

3.3. Microstructural Studies of Ni Coatings

Studying the morphology of coatings using SEM allows to find out that pure nickel is characterized by a disordered amorphous surface (Figure 6a), while the microstructure of Ni–NMGO MMC is dense and finely crystalline (Figure 6b). Therefore, it can be assumed that particles of nitrogen-modified graphene oxide act as crystallization centers during the formation of a nickel deposit and contribute to its uniform distribution over the cathode surface.

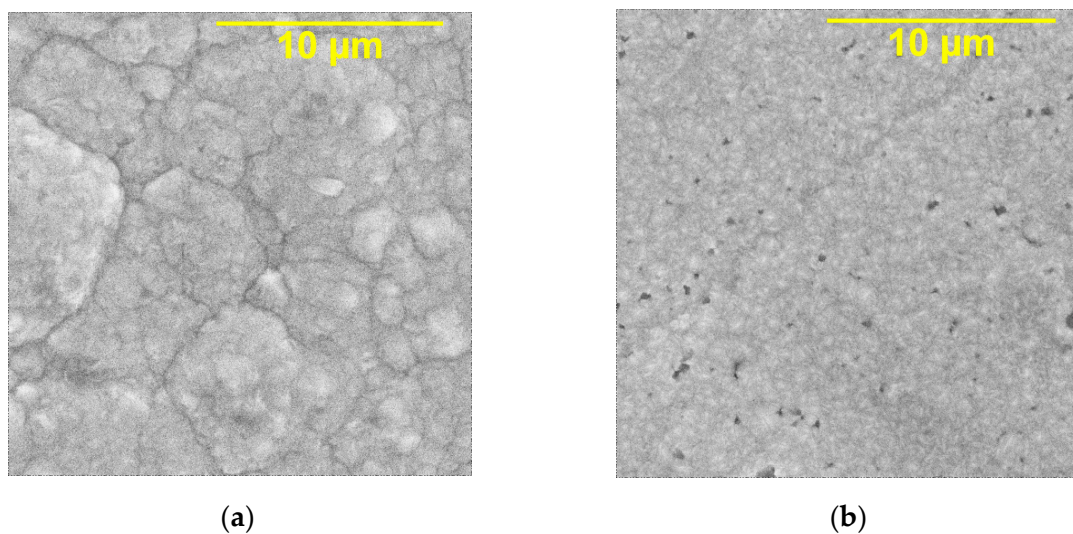


Figure 6. SEM images of Ni (a) and Ni–NMGO MMC (b), deposited at $i_c = 10 \text{ A/dm}^2$ (magnification $\times 10,000$).

X-ray phase analysis (XPA) of Ni coating and Ni–NMGO MMC shows that under the influence of a dispersed additive of nitrogen-modified graphene oxide, a significant change in the crystalline structure of nickel occurs. The peak in the diffraction pattern of pure nickel at 39° corresponds to the direction of growth of the nickel crystal lattice towards the plane (100), the peak at 44° corresponds to the plane (111), and the peaks at 52° and 67° indicate the growth of the nickel crystal in the direction of the plane (200) (Figure 7). Another peak in the diffraction pattern at 65° is likely to correspond to the (220) plane, which under normal conditions is formed at 76° , but due to residual stresses in the crystal, its shift could occur. In the presence of NMGO, the nickel crystal lattice undergoes some changes in growth. In both cases, the preferable orientation of the lattice growth is towards the (111) plane; however, in the case of MMC, the intensity of growth in this direction increases significantly. A similar increase in peak intensity is observed at 39° , 52° , and 67° in the direction of the (100) and (200) planes. The appearance of a carbon peak in the diffraction pattern of Ni–NMGO MMC confirms the inclusion of a dispersed phase of nitrogen-modified graphene oxide in the Ni matrix.

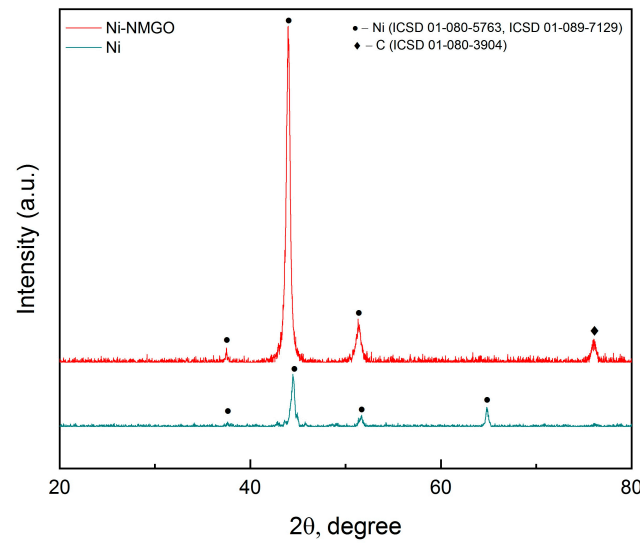


Figure 7. XRD patterns of Ni and Ni–NMGO MMC obtained at $i_c = 10 \text{ A/dm}^2$.

3.4. Microhardness

Particles of the dispersed phase, penetrating into the metal matrix, not only change the structure of the forming MMCs, but also affect their functional properties. One of the important applied characteristics of electrochemical coatings is their microhardness. Studies have shown that the Vickers microhardness of Ni–GO coatings increases by 1.20 times whereas this parameter of Ni–NMGO MMCs increases on average by 1.30 times compared to unmodified Ni deposits (Table 2). Obviously, the identified effect is a consequence of several factors at once. First of all, it is necessary to highlight the refinement of crystallites, leading to dispersion strengthening of the Ni matrix in the presence of particles of nitrogen-modified graphene oxide (Figure 5). The crystallite size of the studied coatings was calculated based on the XPA data (Figure 6) at the intensity of the crystal lattice (111) according to Scherrer’s Equation [35]:

$$d = \frac{0.9\lambda}{b\cos\theta} \tag{1}$$

where d is the crystallite size, λ is the wavelength of the radiation used ($\lambda = 0.15412 \text{ nm}$), θ is the diffraction angle, b is the full-width half maximum at the peak of 2θ .

Table 2. Microhardness $HV_{0.10}$ in MPa of Ni coatings.

Cathode Current Density i_c , A/dm ²	Ni	Ni–GO	Ni–NMGO
7	1938	2200	2350
8	2150	2520	2639
9	2350	2938	3140
10	2459	3076	3235

Calculations show that the crystallite size decreases from 69.0 nm in the case of Ni without the dispersed phase to 18.4 nm for Ni–NMGO MMC, i.e., 3.75 times. Due to the refinement of crystallites, the length of grain boundaries increases, which prevents the movement of dislocations and other stacking faults along the crystal lattice. Secondly, it should be noted that NMGO particles embedded in the Ni matrix have high mechanical properties and are distributed predominantly along grain boundaries, acting as a barrier to the propagation of slip planes. In addition, the inclusion of the dispersed phase of nitrogen-modified graphene oxide in the coating leads to the effect of strengthening thin crystals.

3.5. Corrosion Studies

In addition to mechanical strength, anti-corrosion properties of electrolytic deposits are of significant practical importance. The corrosion-electrochemical behavior of nickel coatings was studied by recording anodic potentiodynamic curves in a 0.5 M sulfuric acid solution. Analysis of chronovoltammograms (Figure 8) shows a notable broadening of the passive region of Ni–NMGO MMC compared to electrochemical Ni not modified by the dispersed phase. In general, the rate of anodic dissolution of the metal depends slightly on the potential value and changes insignificantly when E shifts to positive values. Obviously, the broadening of the passive region of the metal matrix coating is determined by the influence of nitrogen-modified graphene oxide. The results of studies in 0.5 M H₂SO₄ let us assume that the rate of corrosion processes on Ni–NMGO MMCs will be lower than on electrolytic deposits of pure Ni.

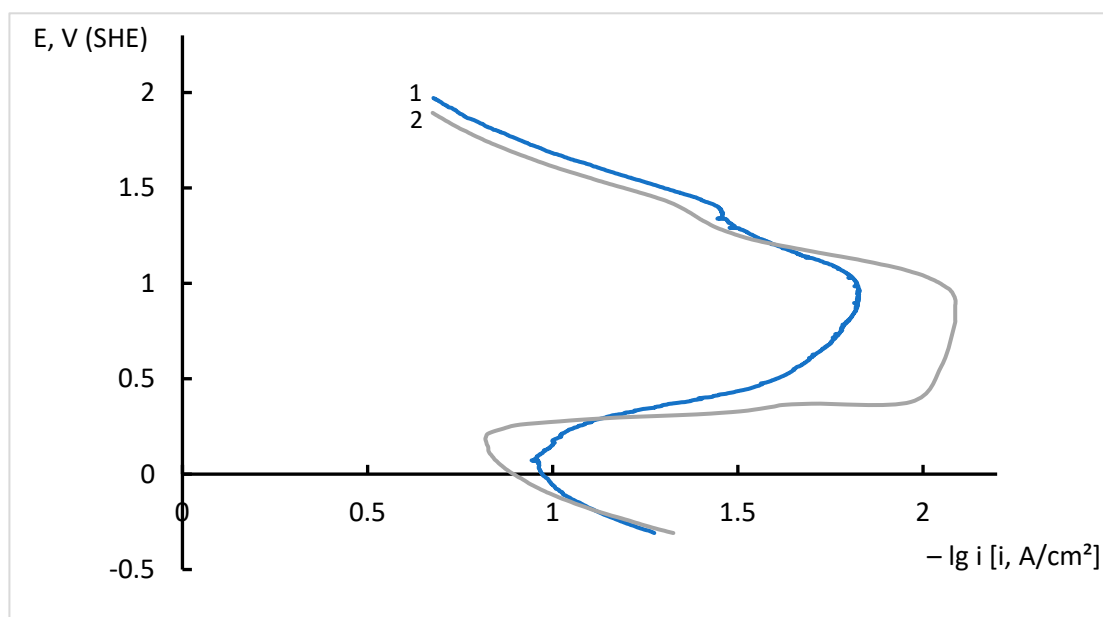


Figure 8. Chronovoltammograms of Ni (1) and Ni–NMGO MMC (2) in 0.5 M H₂SO₄ (coatings obtained at $i_c = 10$ A/dm²).

The corrosion rate was determined by the weight loss of the coatings under study when they were kept in 3.5% NaCl for 24 h (the electrodes were weighed before and after immersion in saline solution) according to the formula [36,37]:

$$\text{Corrosion rate} = \frac{KW}{ATD} \quad (2)$$

where K is constant (8.76×10^4), W is mass loss in g, A is the working surface area of the studied electrodes (1 cm²), T is immersion time in hours, and D is nickel density (8.90 g/cm³).

Tests in the sodium chloride environment showed that the corrosion rate of Ni–NMGO MMCs was reduced by approximately 1.50–1.70 times compared to pure Ni deposits (Table 3). The improvement in the corrosion properties of metal matrix coatings can be explained by the influence of several factors. The nitrogen-modified graphene oxide particles in the nickel matrix will act as a barrier preventing the initiation and propagation of the corrosion process. In addition, they will form corrosive galvanic microelements with Ni, promoting anodic polarization. Since Ni–NMGO MMCs have a fine-crystalline structure (Figure 5), the presence of these trace elements in their composition will contribute to the uniform distribution of the corrosion current over the surface. The susceptibility of an electrochemical coating to corrosion damage also depends on its texture, which determines

the free energy per unit surface area. Closed-packed crystal planes often dissolve faster due to the lower energy required to break the bond (predominant dissolution of metal atoms occurs in a certain direction). According to the XPA data, the (111) planes are more densely packed for the studied nickel coatings than the (200) planes. This probably also contributes to the improvement of the corrosion properties of Ni–NMGO MMCs.

Table 3. Corrosion rates in mm/year of Ni coatings.

Cathode Current Density i_c , A/dm ²	Ni	Ni–GO	Ni–NMGO
7	0.656	0.492	0.430
8	0.574	0.410	0.369
9	0.451	0.328	0.287
10	0.328	0.205	0.185

4. Conclusions

We have developed a method for the production of nitrogen-modified graphene oxide by hydrothermal synthesis in the presence of triethanolamine. It has been shown that by adding NMGO dispersion into the composition of a Watts-type nickel sulfate–chloride electrolyte, metal-matrix coatings are deposited. The modification of electrolytic Ni by NMGO particles resulted in changes in the microstructure and functional properties of the forming MMCs. The surface of Ni–NMGO deposits is fine-crystalline and ordered. The microhardness of Ni–NMGO coatings increases, on average, by 1.30 times, and their corrosion rate decreases by approximately 1.50 times compared to Ni deposits that do not contain NMGO phase. Ni–NMGO MMC obtained at $i_c = 10$ A/dm² has optimal performance properties.

Author Contributions: Conceptualization, V.T.; Data curation, D.T. and A.D.; Formal analysis, A.Y. and A.T.; Investigation, V.T., D.T. and A.D.; Methodology, V.T., A.D., D.T., S.B. and A.Y.; Project administration, V.T.; Supervision, V.T.; Visualization, A.D., A.Y., D.T., A.T., S.B., A.M. and M.L.; Writing—original draft, V.T.; Writing—review and editing, V.T., A.D., D.T., A.Y., S.B., A.T., A.M. and M.L. All authors participated in the discussion of the results and the writing of the text of the article. All authors have read and agreed to the published version of the manuscript.

Funding: This research received no external funding.

Data Availability Statement: Data are contained within the article.

Conflicts of Interest: The authors declare no conflicts of interest.

References

- Orinakova, R.; Turonova, A.; Kladekova, D.; Galova, M.; Smith, R.M. Recent developments in the electrodeposition of nickel and some nickel-based alloys. *J. Appl. Electrochem.* **2006**, *36*, 957–972. [[CrossRef](#)]
- Low, C.T.J.; Wills, R.G.A.; Walsh, F.C. Electrodeposition of composite coatings containing nanoparticles in a metal deposit. *Surf. Coat. Technol.* **2006**, *201*, 371–383. [[CrossRef](#)]
- Tseluikin, V.N. Composite coatings modified with nanoparticles: Structure and properties. *Nanotechnol. Russ.* **2014**, *9*, 1–14. [[CrossRef](#)]
- Walsh, F.C. A review of the electrodeposition of metal matrix composite coatings by inclusion of particles in a metal layer: An established and diversifying technology. *Trans. IMF* **2014**, *92*, 83–98. [[CrossRef](#)]
- Giannopoulos, F.; Chronopoulou, N.; Bai, J.; Zhao, H.; Pantelis, D.; Pavlatou, E.A.I.; Karatonis, A. Nickel/MWCNT–Al₂O₃ electrochemical co-deposition: Structural properties and mechanistic aspects. *Electrochim. Acta* **2016**, *207*, 76–86. [[CrossRef](#)]
- Jyotheender, K.S.; Gupta, A.; Srivastava, C. Grain boundary engineering in Ni-carbon nanotube composite coatings and its effect on the corrosion behaviour of the coatings. *Materialia* **2020**, *9*, 100617. [[CrossRef](#)]
- Yang, P.; Wang, N.; Zhang, J.; Lei, Y.; Shu, B. Investigation of the microstructure and tribological properties of CNTs/Ni composites prepared by electrodeposition. *Mater. Res. Express* **2022**, *9*, 036404. [[CrossRef](#)]
- Antihovich, I.V.; Ablazhey, N.M.; Chernik, A.A.; Zharsky, I.M. Electrodeposition of nickel and composite nickel-fullerenol coatings from low-temperature sulphate-chloride-isobutyrate electrolyte. *Procedia Chem.* **2014**, *10*, 373–377. [[CrossRef](#)]

9. Tseluikin, V.N. Electrodeposition and properties of composite coatings modified by fullerene C₆₀. *Prot. Met. Phys. Chem. Surf.* **2017**, *53*, 433–436. [[CrossRef](#)]
10. Chayeuski, V.V.; Zhylynski, V.V.; Rudak, P.V.; Rusalsky, D.P.; Visniakov, N.; Cernasejus, O. Characteristics of ZrC/Ni-UDD coatings for a tungsten carbide cutting tool. *Appl. Surf. Sci.* **2018**, *446*, 18–26. [[CrossRef](#)]
11. Makarova, I.; Dobryden, I.; Kharitonov, D.; Kasach, A.; Ryl, J.; Repo, E.; Vuorinen, E. Nickel-nanodiamond coatings electrodeposited from tartrate electrolyte at ambient temperature. *Surf. Coat. Technol.* **2019**, *380*, 125063. [[CrossRef](#)]
12. Algul, H.; Tokur, M.; Ozcan, S.; Uysal, M.; Cetinkaya, T.; Akbulut, H.; Alp, A. The effect of graphene content and sliding speed on the wear mechanism of nickel–graphene nanocomposites. *Appl. Surf. Sci.* **2015**, *359*, 340–348. [[CrossRef](#)]
13. Yasin, G.; Arif, M.; Nizam, N.M.; Shakeel, M.; Khan, M.A.; Khan, W.Q.; Hassan, T.M.; Abbas, Z.; Farahbakhsh, I.; Zuo, Y. Effect of surfactant concentration in electrolyte on the fabrication and properties of nickel-graphene nanocomposite coating synthesized by electrochemical co-deposition. *RSC Adv.* **2018**, *8*, 20039–20047. [[CrossRef](#)] [[PubMed](#)]
14. Ambrosi, A.; Pumera, M. The structural stability of graphene anticorrosion coating materials is compromised at low potentials. *Chem.-A Eur. J.* **2015**, *21*, 7896–7901. [[CrossRef](#)] [[PubMed](#)]
15. Jyotheender, K.S.; Srivastava, C. Ni-graphene oxide composite coatings: Optimum graphene oxide for enhanced corrosion resistance. *Compos. Part B* **2019**, *175*, 107145. [[CrossRef](#)]
16. Tseluikin, V.; Dzhumieva, A.; Tikhonov, D.; Yakovlev, A.; Strilets, A.; Tribis, A.; Lopukhova, M. Pulsed electrodeposition and properties of nickel-based composite coatings modified with graphene oxide. *Coatings* **2022**, *12*, 656. [[CrossRef](#)]
17. Tseluikin, V.; Dzhumieva, A.; Yakovlev, A.; Tikhonov, D.; Tribis, A.; Strilets, A.; Lopukhova, M. Electrodeposition and Properties of Composite Ni Coatings Modified with Multilayer Graphene Oxide. *Micromachines* **2023**, *14*, 1747. [[CrossRef](#)] [[PubMed](#)]
18. Korkmaz, S.; Kariper, İ.A. Graphene and graphene oxide based aerogels: Synthesis, characteristics and supercapacitor applications. *J. Energy Storage* **2020**, *27*, 101038. [[CrossRef](#)]
19. Arvas, M.B.; Gürsu, H.; Gencten, M.; Sahin, Y. Preparation of different heteroatom doped graphene oxide based electrodes by electrochemical method and their supercapacitor applications. *J. Energy Storage* **2021**, *35*, 102328. [[CrossRef](#)]
20. Yadav, R.; Subhash, A.; Chemmenchery, N.; Kandasubramanian, B. Graphene and graphene oxide for fuel cell technology. *Ind. Eng. Chem. Res.* **2018**, *57*, 9333–9350. [[CrossRef](#)]
21. Tian, Y.; Yu, Z.; Cao, L.; Zhang, X.L.; Sun, C.; Wang, D.W. Graphene oxide: An emerging electromaterial for energy storage and conversion. *J. Energy Chem.* **2021**, *55*, 323–344. [[CrossRef](#)]
22. Joshi, D.J.; Koduru, J.R.; Malek, N.I.; Hussain, C.M.; Kailasa, S.K. Surface modifications and analytical applications of graphene oxide: A review. *TrAC Trends Anal. Chem.* **2021**, *144*, 116448. [[CrossRef](#)]
23. Gholampour, A.; Valizadeh Kiamahalleh, M.; Tran, D.N.; Ozbakkaloglu, T.; Losic, D. From graphene oxide to reduced graphene oxide: Impact on the physiochemical and mechanical properties of graphene–cement composites. *ACS Appl. Mater. Interfaces* **2017**, *9*, 43275–43286. [[CrossRef](#)] [[PubMed](#)]
24. Carboni, N.; Mazzapioda, L.; Capri, A.; Gatto, I.; Carbone, A.; Baglio, V.; Navarra, M.A. Composite Anion Exchange Membranes based on Graphene Oxide for Water Electrolyzer Applications. *Electrochim. Acta* **2024**, *486*, 144090. [[CrossRef](#)]
25. Priyadarsini, S.; Mohanty, S.; Mukherjee, S.; Basu, S.; Mishra, M. Graphene and graphene oxide as nanomaterials for medicine and biology application. *J. Nanostruct. Chem.* **2018**, *8*, 123–137. [[CrossRef](#)]
26. Gupta, A.; Srivastava, C. Enhanced corrosion resistance by SnCu-graphene oxide composite coatings. *Thin Solid Films* **2019**, *669*, 85–95. [[CrossRef](#)]
27. Lai, R.; Shi, P.; Yi, Z.; Li, H.; Yi, Y. Triple-band surface plasmon resonance metamaterial absorber based on open-ended prohibited sign type monolayer graphene. *Micromachines* **2023**, *14*, 953. [[CrossRef](#)] [[PubMed](#)]
28. Chen, Z.; Cai, P.; Wen, Q.; Chen, H.; Tang, Y.; Yi, Z.; Wei, K.; Li, G.; Tang, B.; Yi, Y. Graphene multi-frequency broadband and ultra-broadband terahertz absorber based on surface plasmon resonance. *Electronics* **2023**, *12*, 2655. [[CrossRef](#)]
29. Khanari, K.; Grah, N.; Finšgar, M.; Fuchs-Godec, R.; Maver, U. Corrosion inhibition and surface analysis of amines on mild steel in chloride medium. *Chem. Pap.* **2017**, *71*, 81–89. [[CrossRef](#)]
30. Muhsin, M.S.; Shihab, M.S. Synthesis New Triethylammonium salts as corrosion inhibitors for mild steel in 1 M H₂SO₄. *Al-Nahrain J. Sci.* **2023**, *26*, 6–18. [[CrossRef](#)]
31. Shang, W.; He, C.; Wen, Y.; Wang, Y.; Zhang, Z. Performance evaluation of triethanolamine as corrosion inhibitor for magnesium alloy in 3.5 wt% NaCl solution. *RSC Adv.* **2016**, *6*, 113967–113980. [[CrossRef](#)]
32. Ban, C.G.; Zhang, K.; Huang, L.; Yuan, Y. Triethanolamine modified graphene oxide for epoxy resin-based coatings: Corrosion inhibition on metal substrates. *Surf. Interface Anal.* **2022**, *54*, 1151–1162. [[CrossRef](#)]
33. Yakovlev, A.V.; Yakovleva, E.V.; Vikulova, M.A.; Frolov, I.N.; Rakhmetulina, L.A.; Tseluikin, V.N.; Krasnov, V.V.; Mostovoy, A.S. Synthesis of multilayer graphene oxide in electrochemical graphite dispersion in H₂SO₄. *Russ. J. Appl. Chem.* **2020**, *93*, 219–224. [[CrossRef](#)]
34. Muzyka, R.; Drewniak, S.; Pustelny, T.; Chrubasik, M.; Gryglewicz, G. Characterization of graphite oxide and reduced graphene oxide obtained from different graphite precursors and oxidized by different methods using Raman Spectroscopy. *Materials* **2018**, *11*, 1050. [[CrossRef](#)] [[PubMed](#)]
35. Zhang, H.; Zhang, N.; Fang, F. Fabrication of high-performance nickel/graphene oxide composite coatings using ultrasonic-assisted. *Ultrason. Sonochem.* **2020**, *62*, 104858. [[CrossRef](#)] [[PubMed](#)]

36. Rekha, M.Y.; Srivastava, C. Microstructural evolution and corrosion behavior of Zn-Ni-graphene oxide composite coatings. *Metall. Mater. Trans. A* **2019**, *50*, 5896–5913. [[CrossRef](#)]
37. Yang, F.; Kang, H.; Guo, E.; Li, R.; Chen, Z.; Zeng, Y. The role of nickel in mechanical performance and corrosion behaviour of nickel-aluminium bronze in 3.5 wt.% NaCl solution. *Corros. Sci.* **2018**, *139*, 333–345. [[CrossRef](#)]

Disclaimer/Publisher's Note: The statements, opinions and data contained in all publications are solely those of the individual author(s) and contributor(s) and not of MDPI and/or the editor(s). MDPI and/or the editor(s) disclaim responsibility for any injury to people or property resulting from any ideas, methods, instructions or products referred to in the content.